Density functional theory study on the B doping and B/P codoping of Si nanocrystals embedded in SiO_2

Zhenyi Ni (倪朕伊),[1] Xiaodong Pi (皮孝东),[1,*] Stefaan Cottenier,[2] and Deren Yang (杨德仁)[1,†]

[1] *State Key Laboratory of Silicon Materials and School of Materials Science and Engineering, Zhejiang University, Hangzhou, Zhejiang 310027, China*

[2] *Center for Molecular Modeling and Department of Materials Science and Engineering, Ghent University, Technologiepark 903, BE-9052 Zwijnaarde, Belgium*

(Received 22 October 2016; revised manuscript received 19 January 2017; published 21 February 2017)

Doping silicon nanocrystals (Si NCs) embedded in silicon dioxide (SiO_2) with boron (B) and phosphorus (P) is a promising way of tuning the properties of Si NCs. Here we take advantage of density functional theory to investigate the dependence of the structural and electronic properties of Si NCs embedded in SiO_2 on the doping of B and P. The locations and energy-level schemes are examined for singularly B-doped or B/P-codoped Si NCs embedded in SiO_2 with a perfect or defective Si/SiO_2 interface at which a Si dangling bond exists. A dangling bond plays an important role in the doping of Si NCs with B or B/P. The doping behavior of B in Si NCs embedded in SiO_2 vastly differs from that of P. The electronic structure of a B/P-codoped Si NC largely depends on the distribution of the dopants in the NC.

DOI: 10.1103/PhysRevB.95.075307

I. INTRODUCTION

Silicon nanocrystals (Si NCs) have been intensively investigated during past decades for their promising applications in various fields such as optoelectronics [1–6], photovoltaics [7–11], energy storage [12,13], and bioimaging [14,15]. This is mainly due to their nontoxicity, low cost, and compatibility with well-established Si-based microelectronic technology. It has been recently shown that doping is a critical means to realize the full potential of Si NCs [16–19]. For example, low-energy light emission related to the transitions of electrons from the band edge to the defect state has been observed in boron (B)- and phosphorus (P)-doped Si NCs [20–23], leading to enhanced tunability of the light emission from Si NCs. In addition, heavy B and P doping have enabled localized surface plasmon resonance (LSPR) for Si NCs [24–28]. A series of novel devices that take advantage of the doping-induced properties of Si NCs are now highly expected. Among a variety of matrices in which Si NCs can be embedded, SiO_2 is very popular because of the excellent availability of SiO_2 and the high-quality interface between Si NCs and SiO_2 [29–31]. Therefore, the doping of Si NCs embedded in SiO_2 deserves careful investigation during the course of advancing Si-NC-based technology.

In contrast to the doping of hydrogen-passivated Si NCs, the doping of Si NCs embedded in SiO_2 has not been systematically simulated because complicated models need to be used in the simulation [32–35]. Guerra and Ossicini [36] and Carvalho *et al.* [37] investigated the doping of B and P in Si NCs that were passivated by OH groups. However, the absence of the Si/SiO_2 interface in their OH-terminated Si NC models was somehow far away from the routinely encountered situation. We have recently managed to simulate the P doping of Si NCs embedded in SiO_2 by constructing SiO_2-coated Si NCs [38]. The results highlighted the difference in the distribution of P and the electronic properties between hydrogen-passivated Si NCs and those with oxide at the surface [38,39]. Now we further investigate the B doping and B/P codoping of Si NCs embedded in SiO_2 in the framework of density functional theory (DFT). The model of a Si NC embedded in SiO_2 (Si@SiO_2) is constructed by coating a 1.4-nm Si NC with a monolayer of SiO_2 (0.25 nm thick), which is itself passivated by hydrogen. It has been already demonstrated that the rather thin SiO_2 layer is able to model the matrix-induced strain as well as the defective Si/SiO_2 interface [38,40]. For all NC models that are constructed this way, a full geometry optimization is performed. The locations and energy-level schemes are examined for B-doped or B/P-codoped Si NCs embedded in SiO_2 with a perfect or defective Si/SiO_2 interface. It is found that the B doping vastly differs from the P doping for Si NCs embedded in SiO_2. We also show that the electronic structures of B/P-codoped Si NCs embedded in SiO_2 are closely related to the distribution of the dopants.

II. METHOD

The optimization of structures and the calculation of total energies are performed at 0 K by using the all-electron DFT modeling package DMol3 [38,41,42]. The Becke-Lee-Yang-Parr (BLYP) exchange-correlation functional at the generalized gradient approximation (GGA) level is used. Double numerical basis sets augmented with *p*-polarization functions (DNP basis sets) are employed as the atomic orbital basis functions. To ensure accurate calculation, a high self-consistent field (SCF) convergence threshold of 10^{-6} and a large orbital cutoff of 4.6 Å are employed. The maximum energy change and forces on all of the atoms in the optimized structures are less than 10^{-5} Ha and 0.002 Ha/Å, respectively. To prevent the optimizer from taking unreasonable steps, the maximum allowed change of any Cartesian coordinate during the structural relaxation is less than 0.3 Å. The highest occupied molecular orbital (HOMO), highest occupied deep energy level (HODE), lowest unoccupied deep energy level (LUDE), and lowest unoccupied molecular orbital (LUMO) are sampled on a grid with a spacing of 0.2 A.

*Corresponding author: xdpi@zju.edu.cn
†Corresponding author: mseyang@zju.edu.cn

 ©2017 American Physical Society

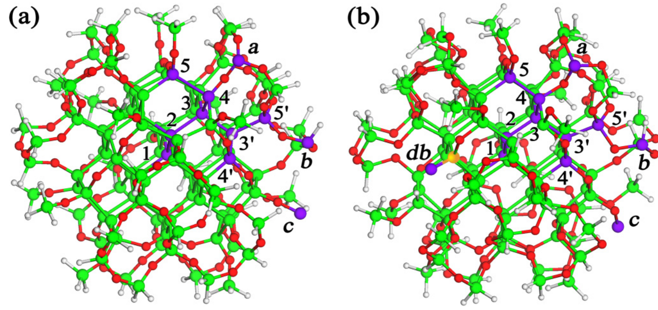

FIG. 1. Model of an optimized 1.4-nm Si NC embedded in SiO_2 with an (a) perfect Si/SiO_2 interface ($Si@SiO_2$, $Si_{123}H_{100}O_{96}$) or (b) defective Si/SiO_2 interface at which a Si dangling bond exists ($Si@_{db}SiO_2$, $Si_{123}H_{101}O_{95}$). Si, H, and O atoms are denoted by green, gray, and red balls, respectively. A Si atom initially with a dangling bond at the Si/SiO_2 interface is highlighted by an orange ball. A substitutional or passivating B atom is indicated by a violet ball. B1, B2, B3 (B3′), B4 (B4′), and B5 (B5′) result from moving a substitutional B atom along the path of 1 → 2 → 3 (3′) → 4 (4′) → 5 (5′). When a B atom replaces a Si atom connected to one, two, or three H atoms at the surface, it is denoted as B_a, B_b, or B_c, respectively. As a B atom passivates a Si dangling bond at the Si/SiO_2 interface, it is denoted as B_{db}.

III. B DOPING

A. Formation energy

Figure 1 shows the model of a geometry-optimized 1.4-nm Si NC embedded in SiO_2 with (a) perfect Si/SiO_2 interface ($Si@SiO_2$) or (b) defective Si/SiO_2 interface at which a Si dangling bond exists ($Si@_{db}SiO_2$). The model of $Si@SiO_2$ is based on a 1.4-nm H-passivated Si NC (Si@H, $Si_{71}H_{84}$), which has been detailed in our previous work [43–47]. An O atom is used to replace every H atom in SiH and SiH_3 at the surface of Si@H, which is then outwardly bonded to an added Si atom. One O atom is inserted bewteen two Si atoms in the neighboring SiH_2 due the fact that the room between neighboring SiH_2 may be too small to accommodate both added O and Si. H atoms are used to passivate the remaining dangling bonds at the surface of the NC. When a Si dangling bond is considered at the Si/SiO_2 interface, one O atom is removed at the interface. This gives rise to three types of dangling bonds, i.e., $\cdot Si{\equiv}(SiO_2)$, $\cdot Si{\equiv}(Si_2O)$, and $\cdot Si{\equiv}Si_3$ [33,34,48]. We have calculated the formation energies of the dangling bonds with these three configurations. It turns out that the formation energies of $\cdot Si{\equiv}(SiO_2)$, $\cdot Si{\equiv}(Si_2O)$, and $\cdot Si{\equiv}Si_3$ are 4.6, 2.8, and 5.7 eV, respectively. Since the formation energy of $\cdot Si{\equiv}(Si_2O)$ is the lowest, the dangling bond is the most likely in the configuration of $\cdot Si{\equiv}(Si_2O)$. Therefore, we only consider the Si dangling bond of $\cdot Si{\equiv}(Si_2O)$ in the current work. Although the thickness of the SiO_2 layer at the NC surface is only ~0.25 nm, the SiO_2-induced strain and reduction of the NC band gap are similar to what Seino *et al.* [40,49] have demonstrated for Si NCs embedded in the SiO_2 matrax with a rather conplicated model. This indicates the rationality of our models.

A series of substitutional locations of B for the doping of $Si@SiO_2$ and $Si@_{db}SiO_2$ with B [Figs. 1(a) and 1(b)] are considered. A substitutional B atom that moves along the path of 1 → 2 → 3 (3′) → 4 (4′) → 5 (5′) is denoted as B1, B2, B3 (B3′), B4 (B4′), or B5 (B5′). When a B atom replaces a Si atom that is originally connected to one, two, or three H atoms at the surface of $Si@SiO_2$ or $Si@_{db}SiO_2$, it is denoted as B_a, B_b or B_c, respectively. B_a, B_b, and B_c are passivated by zero, one, and zero H atoms, respectively. As a B atom passivates a Si dangling bond at the Si/SiO_2 interface, it is denoted as B_{db}.

We have calculated the formation energy (E_f) of a B atom in $Si@SiO_2$ or $Si@_{db}SiO_2$ by using [50,51]

$$E_f = E(Si_{x'}O_{y'}H_{z'}B) - E(Si_xO_yH_z) - \mu_B - (x' - x)\mu_{Si} - (y' - y)\mu_O - (z' - z)\mu_H, \quad (1)$$

where $E(Si_xO_yH_z)$ and $E(Si_{x'}O_{y'}H_{z'}B)$ are the total energy of $Si@SiO_2$ or $Si@_{db}SiO_2$ before and after the incorpation of a B atom, respectively. $x(x'), y(y')$, and $z(z')$ are the numbers of Si, O, and H atoms, respectively. μ_{Si}, μ_O, μ_H, and μ_B are the chemical potentials of Si, O, H, and B, respectively. The relative order of E_f for B in all kinds of configurations is not affected by the chemical potentials in a rather wide range given the linear relationship between E_f and each chemical potential. Thus we obtain the values of E_f by choosing μ_{Si}, μ_O, μ_H, and μ_B to equal the total energies of atomic Si, O, H, and B in bulk Si, oxygen gas, hydrogen gas, and B_{12}, respectively [52,53].

Figure 2 shows the values of E_f with respect to the location of B in (a) $Si@SiO_2$ or (b) $Si@_{db}SiO_2$. It is seen that the values of E_f for B at the Si/SiO_2 interface and the surface of $Si@SiO_2$ [i.e., the locations of 4 (4′), 5 (5′), *a* and *b*] are close to those for B in the NC core [Fig. 2(a)]. This result is quite different from that for P-doped $Si@SiO_2$, in which a P atom in the core shows a lower E_f compared with that at the Si/SiO_2 interface and the surface of $Si@SiO_2$ [38]. Such a difference may be due to the fact that the electronegativity of B is weaker than that of P. Attractive interaction between B and O is larger than that between P and O. The minimum value of E_f (–5.6 eV) appears when B is incorporated as B3′ in the subinterface region, indicating that B is the most likely doped at the subinterface region. This is in contrast to the doping of Si@H with B, where B prefers residing at the surface of Si@H [54].

Figure 2(b) shows the dependence of E_f on the location of B for $Si@_{db}SiO_2$. It is noticed that the value of E_f for B5 at the Si/SiO_2 interface is the lowest (−6.1 eV), implying that the Si/SiO_2 interface is more energetically favored for B

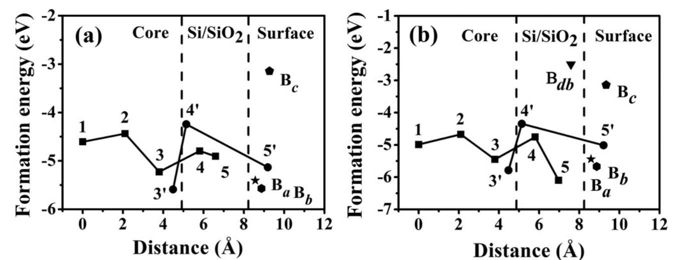

FIG. 2. Formation energy of B in (a) $Si@SiO_2$ or (b) $Si@_{db}SiO_2$ as a B atom substitutionally moves from the center to the surface. The solid lines are used to guide the eye. The vertical dashed lines indicate the regions of the core, Si/SiO_2 interface, and surface.

when a dangling bond exists at the Si/SiO_2 interface. Since dangling bonds often exist at the Si/SiO_2 interface in the real world [55], our current result predicts that B may be routinely found to preferentially occupy the Si/SiO_2 interface region when a Si NC embedded in SiO_2 is doped with B. Khelifi *et al.* [56] and Xie *et al.* [57] have recently demonstrated that this is indeed the case. The existence of a dangling bond at the Si/SiO_2 interface also reduces the values of E_f for B in the NC core [Fig. 2(b)], which means that defects such as Si dangling bonds at the Si/SiO_2 interface may facilitate the incorporation of B for Si NCs embedded in SiO_2. In contrast to P-doped Si@$_{db}$$SiO_2$ [38], B is the least likely to passivate dangling bonds in Si@$_{db}$$SiO_2$. This is consistent with Fujio *et al.*'s [55] experimental work on B-doped Si NCs embedded in SiO_2. They showed that the electron spin resonance (ESR) signal of dangling bonds remains after Si NCs are doped with B.

B. Electronic structure

Figure 3 shows the energy-level diagrams for undoped and B-doped (a) Si@SiO_2 or (b) Si@$_{db}$$SiO_2$. For Si@$SiO_2$, deep energy levels are introduced in the band gap when B is in the configurations of B1, B2, B3 (B3′), B4 (B4′), and B5 (B5′). This is mainly due to the B-doping-induced odd number of electrons in a NC. Among these configurations, the B-doping-induced deep energy levels of B1, B2, B3, and B3′ are close to the valence band with a small spin splitting, while those of B4, B4′, B5, and B5′ are deep with a large spin splitting. The spin splitting of the deep energy level is associated with the polarizability of bonds, which is determined by the variation of the bond length. For B-doped Si@SiO_2 with the configurations of B1, B2, B3, and B3′, the bond lengths of four Si-B bonds are almost identical with each other, giving rise to rather small polarization of the bonds. In these cases, the electron density of the HODE and LUDE are mainly located at the B and neighboring Si atoms with similar distributions [representatively shown for Si@SiO_2 doped with B3′ in Fig. 4(a)]. However, there are significant changes of bond length when B is doped in the configurations of B4, B4′, B5, and B5′. For example, for B-doped Si@SiO_2 with the configuration of B5, the bond length of a Si-B bond is stretched by 60% and that of the adjacent Si-B bond is compressed by 10%. For B5′-doped Si@SiO_2, the B atom even moves to the NC surface after structural optimization [Fig. 1(a)], creating a Si dangling bond at the Si/SiO_2 interface. In these cases, the electron density of the HODE and LUDE are mainly localized at the B atom and adjacent Si dangling bond with divergent distributions [representatively shown for Si@SiO_2 doped with B5 in Fig. 4(a)]. It is the strong localization and divergent distribution of the electron density of HODE and LUDE that contributes to the deep energy levels and large spin splitting, respectively.

The band gap of undoped Si@SiO_2 is slightly enlarged when a dangling bond exists at the Si/SiO_2 interface (1.59 → 1.66 eV). In the meantime, the dangling bond introduces deep energy levels in the band gap, which is evidenced by the fact that the electron density of the HODE and LUDE of Si@$_{db}$$SiO_2$ are mainly localized at the dangling bond [Fig. 4(b)]. For Si@$_{db}$$SiO_2$ doped with B in the configurations of B1, B2, B3 (B3′), B4 (B4′), and B5 (B5′), deep energy levels remain. Similar to what happens to Si@SiO_2, the bond length is almost unchanged when B is doped in the configurations of B1, B2, B3, and B3′. The electron density of the HODE are localized around B, while those of the LUDE are localized on the dangling bond [representatively shown for Si@$_{db}$$SiO_2$ doped with B3′ in Fig. 4(b)]. We find that the single electron of the original dangling bond is transferred to form an electron pair together with that of a B atom. The electron pair occupies the HODE with opposite spins, consistent with Pauli's exclusion principle. For the configurations of B4, B4′, B5, and B5′, significant changes of bond length appear. Both the electron density of the HODE and LUDE are localized on the dangling bond and the Si atom with the largest bond length, leading to deeper energy levels in the band gaps of these configurations. In contrast to P-doped Si@$_{db}$$SiO_2$ with the configuration of P_{db} [38], B doping does not eliminate the deep energy levels with the configuration of B_{db} [Fig. 3(b)]. The electron density of the HODE and LUDE are mainly localized on B_{db} [Fig. 4(b)]. The incorporation of B_a, B_b, or B_c hardly changes the energy-level scheme and electron density of the HOMO and LUMO for Si@SiO_2 or Si@$_{db}$$SiO_2$ (Figs. 3 and 4) because B_a, B_b, or B_c is in threefold coordination at the surface without introducing a single electron.

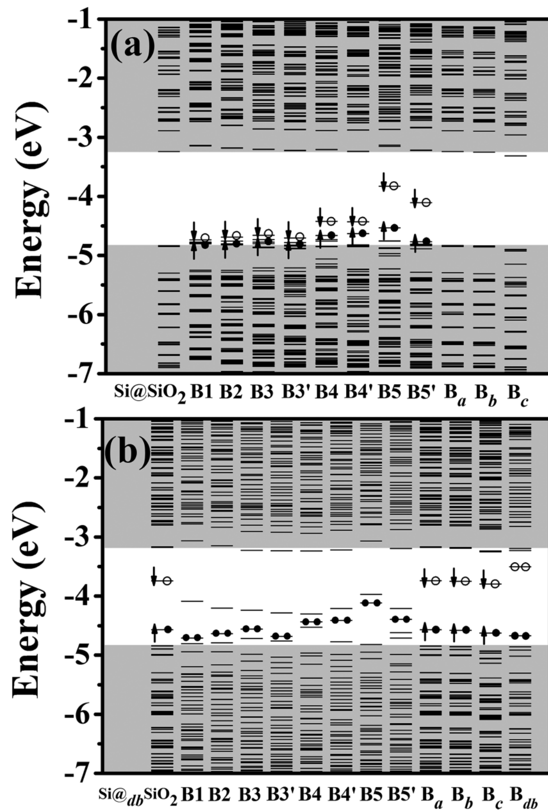

FIG. 3. Energy-level diagrams for undoped and B-doped (a) Si@SiO_2 or (b) Si@$_{db}$$SiO_2$ at the ground state. Filled (empty) circles indicate that energy levels are occupied (unoccupied) by electrons. Spin-up (spin-down) states of defect energy levels induced by a B atom or dangling bond are indicated by up (down) arrows.

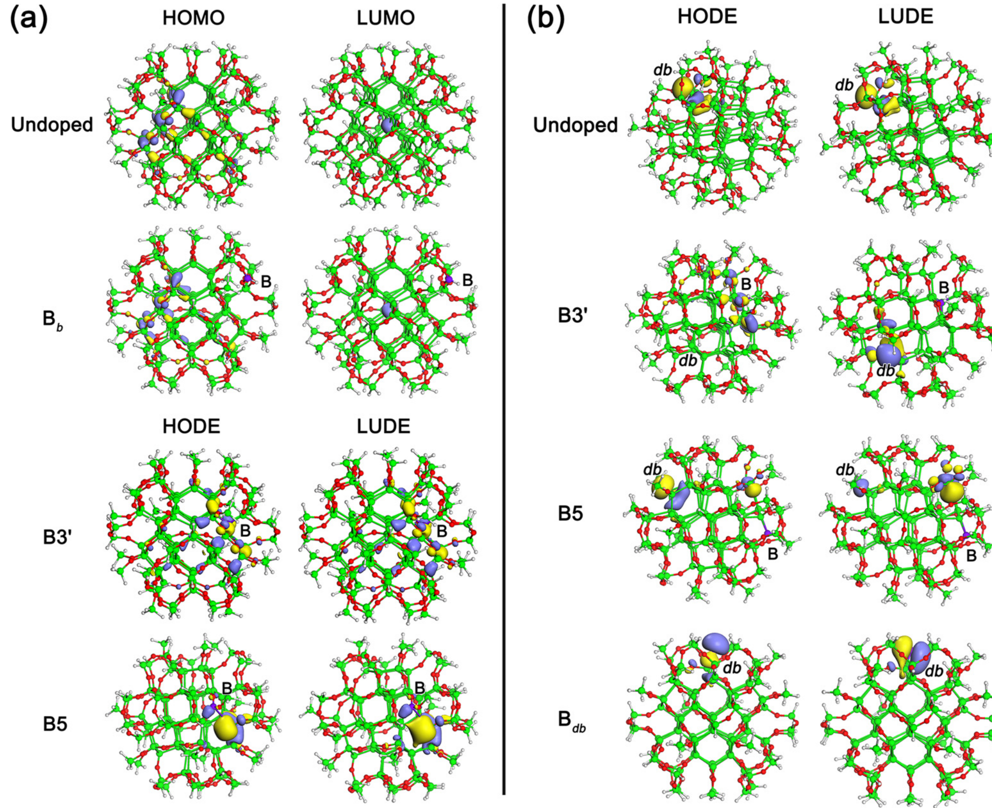

FIG. 4. (a) Distribution of the isosurface for the electron density of the highest occupied molecular orbital (HOMO) and lowest unoccupied molecular orbital (LUMO) for undoped or B_b-doped Si@SiO$_2$. Those of the highest occupied deep energy-level (HODE) and the lowest unoccupied deep energy-level (LUDE) for B3′- or B5-doped Si@SiO$_2$ are also shown. (b) Distribution of the isosurface for the electron density of the HODE and LUDE for undoped, B3′-, B5-, or B_{db}-doped Si@$_{db}$SiO$_2$.

IV. B/P CODOPING

A. Formation energy

Now we focus on the synergic effect of B/P codoping for Si NCs embedded in SiO$_2$. For Si@SiO$_2$, the configurations in which B and P are both incorporated in their energetically favored locations of 3 (3′) at the subinterface region of the NC are first considered [38]. For these configurations, the dopants can either be located separately (denoted as P3-B3′) or form a B-P pair (denoted as {P3-B3′} or {P3′-B3}). In order to figure out which atom is more likely to be incorporated into the core region of the NC when it is codoped with B and P, the configuration of P1-B3′ or P3′-B1 with a P or B atom in the center of the NC is representatively considered. For Si@$_{db}$SiO$_2$, given the result that P is the most likely to passivate the dangling bond at the Si/SiO$_2$ interface [38]. the dangling bond is first passivated by a P atom. A substitutional B atom moving along the path of $1 \rightarrow 2 \rightarrow 3 \rightarrow 4 \rightarrow 5$ is considered. To avoid any strong interaction between the dopants, the path is chosen to be far from P_{db}. These configurations are denoted as P_{db}-B1, P_{db}-B2, P_{db}-B3,P_{db}-B4, and P_{db}-B5. Moreover, a B-P pair in the configuration of {P_{db}-B4′} is considered to investigate the interaction between the dopants for Si@$_{db}$SiO$_2$. Figure 5 shows the models of (a) P3-B3′ codoped Si@SiO$_2$ and (b) P_{db}-B5 codoped Si@$_{db}$SiO$_2$.

The E_f of the dopants in Si@SiO$_2$ or Si@$_{db}$SiO$_2$ is calculated by using

$$E_f = E(\mathrm{Si}_{x'}\mathrm{O}_{y'}\mathrm{H}_{z'}\mathrm{BP}) - E(\mathrm{Si}_x\mathrm{O}_y\mathrm{H}_z) - \mu_\mathrm{B} - \mu_\mathrm{P} - (x'-x)\mu_\mathrm{Si} - (y'-y)\mu_\mathrm{O} - (z'-z)\mu_\mathrm{H}. \quad (2)$$

$E(\mathrm{Si}_x\mathrm{O}_y\mathrm{H}_z)$ and $E(\mathrm{Si}_{x'}\mathrm{O}_{y'}\mathrm{H}_{z'}\mathrm{BP})$ are the total energy of Si@SiO$_2$ or Si@$_{db}$SiO$_2$ before and after the incorpation of B/P dopants, respectively. x (x'), y (y'), and z (z') are the numbers of Si, O, and H atoms, respectively. μ_P is the chemical potential

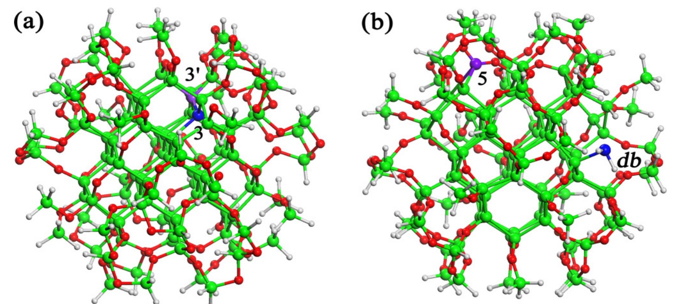

FIG. 5. Model of a (a) Si@SiO$_2$ codoped with P3 and B3′ or (b) Si@$_{db}$SiO$_2$ codoped with P_{db} and B5. Si, H, O, B, and P atoms are denoted by green, gray, red, violet, and blue balls, respectively.

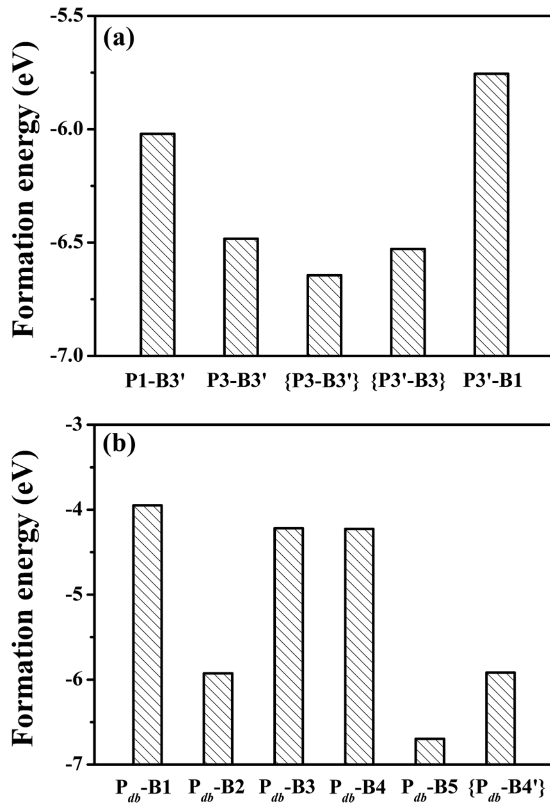

FIG. 6. Formation energies of B/P dopants in (a) Si@SiO_2 or (b) Si@$_{db}SiO_2$.

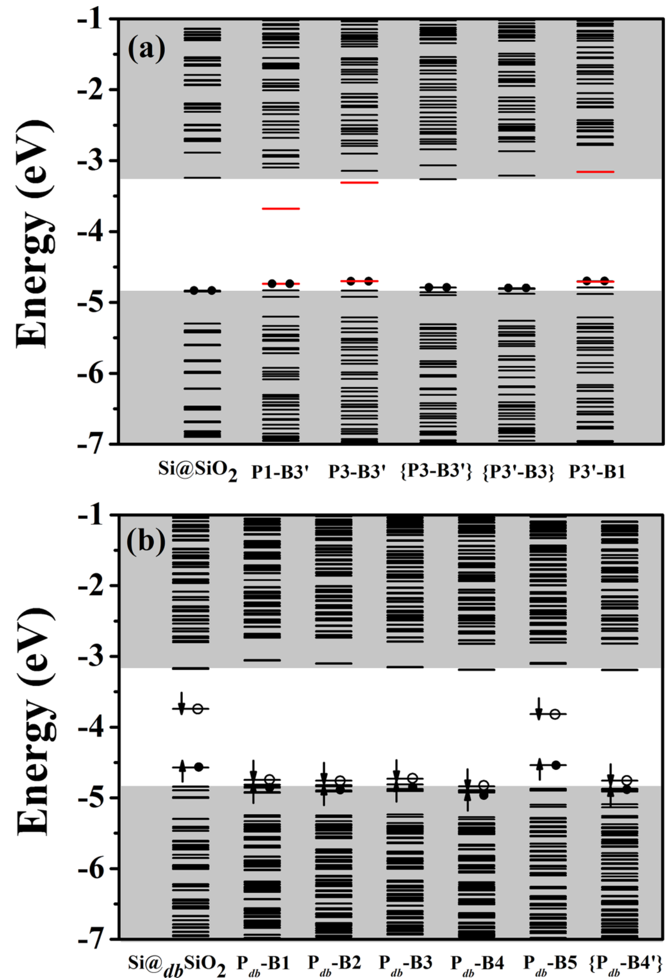

FIG. 7. Energy-level diagrams for undoped and B/P-codoped (a) Si@SiO_2 or (b) Si@$_{db}SiO_2$ at the ground state. Filled (empty) circles indicate that energy levels are occupied (unoccupied) by electrons. Spin-up (spin-down) states of defect energy levels are indicated by up (down) arrows. The highest occupied deep energy-level (HODE) and lowest unoccupied deep energy-level (LUDE) are indicated by red bars.

of P, which equals the total energy of atomic P in orthorhombic black phosphorus [39].

Figure 6 shows the dependence of E_f on the locations of B/P dopants for (a) Si@SiO_2 or (b) Si@$_{db}SiO_2$. For Si@SiO_2, it is clear that the value of E_f for P3-B3′, {P3-B3′}, or {P3′-B3} is smaller than that for P1-B3′ or P3′-B1 [Fig. 6(a)], indicating that it is more energetically stable when both B and P are incorporated at the subinterface of the NC. The value of E_f is further reduced when B and P atoms are doped in the form of a B-P pair. Interestingly, we find that the value of E_f for B/P in the configuration of {P3-B3′} is smaller than that in the configuration of {P3′-B3} (-6.64 vs -6.53 eV). This is mainly because the position of 3′ is closer to the SiO_2 layer than that of 3. A larger attractive interaction between B and electronegative oxygen atoms makes B more energetically favored towards the SiO_2 layer than P. Therefore, the configuration of {P3-B3′} is more likely to be formed compared to that of {P3′-B3}. The existence of a dangling bond makes a difference for the distribution of B and P in Si@$_{db}SiO_2$. For Si@$_{db}SiO_2$, the lowest value of E_f occurs in the configuration of P_{db}-B5, rather than {P_{db}-B4′} [Fig. 6(b)]. This means that B and P are more likely incorporated at the Si/SiO_2 interface of Si@$_{db}SiO_2$ but not in the form of a B-P pair. For both Si@SiO_2 and Si@$_{db}SiO_2$, B is not likely incorporated in the center of the NCs during the codoping of B and P, given the highest values of E_f for the configurations of P3′-B1 and P_{db}-B1 in Si@SiO_2 and Si@$_{db}SiO_2$, respectively.

B. Electronic structure

The energy-level diagrams for undoped and B/P-codoped Si@SiO_2 or Si@$_{db}SiO_2$ are shown in Fig. 7. For Si@SiO_2, deep energy levels are introduced in the band gap when B and P are in the configurations of P1-B3′, P3-B3′, and P3′-B1. The electron density of HODE and LUDE are mainly localized at B and P, respectively. This is representatively shown for Si@SiO_2 codoped with P1-B3′ or P3-B3′ in Fig. 8(a). Figure 9 shows the HODE-LUDE, LUDE-LUMO, and HODE-HOMO gaps for B/P-codoped Si@SiO_2 with the configuration of P1-B3′, P3-B3′, or P3′-B1. It is seen that the band gap between the deep energy levels (HODE-LUDE gap) varies from 1.0 to 1.5 eV for B/P-codoped Si@SiO_2 within these configurations. The LUDE-LUMO gap is much larger than the HODE-HOMO gap for the configurations of P1-B3′ and P3′-B1, while they are almost identical with each other for the configuration of P3-B3′. This demonstrates that the depth of B/P-codoping-induced energy levels is affected by the relative

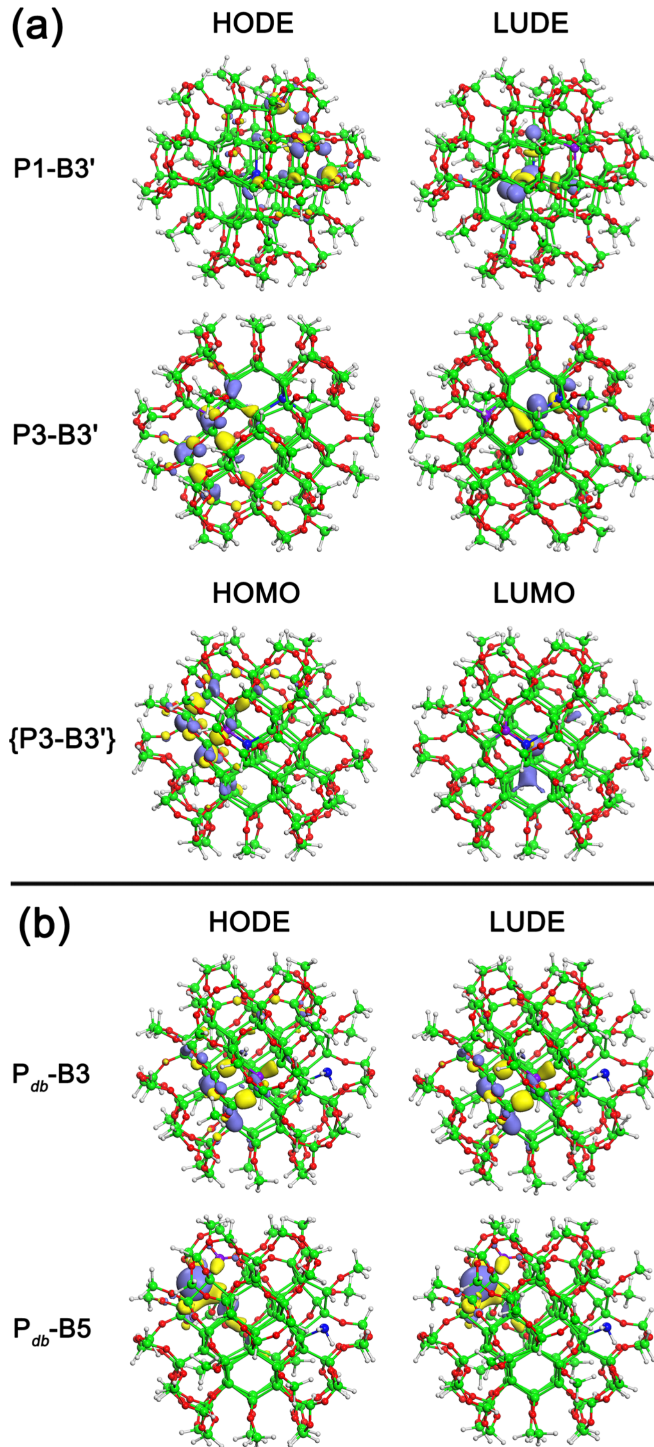

FIG. 8. (a) Distribution of isosurface for the electron density of the HODE and LUDE for P1-B3′ or P3-B3′ codoped Si@SiO_2. Those of the HOMO and LUMO for {P3-B3′} codoped Si@SiO_2 are also shown. (b) Distribution of the isosurface for the electron density of the HODE and LUDE for P_{db}-B3 or P_{db}-B5 codoped Si@$_{db}SiO_2$.

positions of B and P atoms in the NC. Recently, Nakamura *et al.* [31] observed multiphotoluminescence (PL) peaks in heavily B/P-codoped Si NCs embedded in SiO_2. The PL energy of one of the peaks depends on the dopant concentration. These experimental results can be well explained by our current finding that B/P codoping leads to localized states with different depths in the band gap, which are responsible for different PL energies. When B and P atoms are codoped in the form of B-P pairs (i.e., {P3-B3′} and {P3′-B3}), no deep energy levels are introduced in the band gap. The electron density of the HOMO and LUMO are basically delocalized among Si atoms [representatively shown for Si@SiO_2 codoped with {P3-B3′} in Fig. 8(a)].

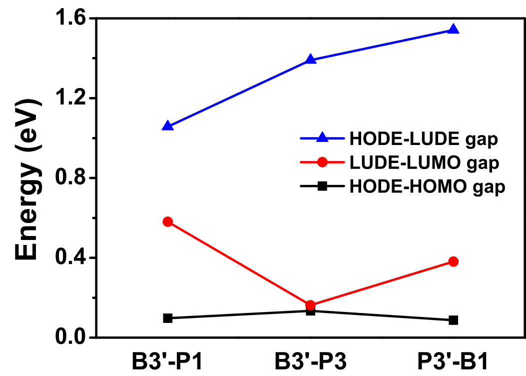

FIG. 9. HODE-LUDE, LUDE-LUMO, and HODE-HOMO gaps for P1-B3′, P3-B3′, or P3′-B1 codoped Si@SiO_2. The solid line is used to guide the eye.

For Si@$_{db}SiO_2$, when a P atom passivates the dangling bond with the configuration of P_{db}, the energy-level scheme of the NC becomes akin to that of undoped Si@SiO_2 [38]. Similar to what happens to Si@SiO_2, the incorporation of an additional B atom in the configurations of B1, B2, B3, B4, B4′, and B5 introduces deep energy levels in the band gap of Si@$_{db}SiO_2$. For B/P-codoped Si@$_{db}SiO_2$ with the configurations of P_{db}-B1, P_{db}-B2, P_{db}-B3, P_{db}-B4, and {P_{db}-B4′}, the electron density of the HODE and LUDE are mainly localized at the B atom [representatively shown for Si@$_{db}SiO_2$ codoped with P_{db}-B3 in Fig. 8(b)]. For P_{db}-B5 codoped Si@$_{db}SiO_2$, significant changes of bond length appear. The electron density of the HODE and LUDE are mainly localized at the B and Si atoms with the largest structural distortion [Fig. 8(b)].

V. CONCLUSIONS

We have studied the B doping and B/P codoping of a Si NC embedded in SiO_2 with a perfect Si/SiO_2 interface (Si@SiO_2) or defective Si/SiO_2 interface (Si@$_{db}SiO_2$). The current results show that B is most likely incorporated into the subinterface of Si@SiO_2. However, the existence of a dangling bond at the Si/SiO_2 interface makes B more energetically prefer the Si/SiO_2 interface. In contrast to the doping of Si@$_{db}SiO_2$ with P, B is not likely to passivate the dangling bond.

For B/P-codoped Si@SiO_2, a B atom and a P atom tend to be bonded as a B-P pair at the subinterface of the NC. A larger electronic attractive interaction between B and O atoms makes B atoms more energetically prefer positions close to the SiO_2 layer. As a consequence, a static electric dipole that radially points toward the NC core is formed at the subinterface region. In fact, B or P may enter the NC core when they are heavily doped. In this case, deep energy levels are introduced in the band gap of Si@SiO_2. The HODE-LUDE gap is affected by the relative positions of B and P atoms.

Finally, we would like to comment on the dependence of the properties of B-doped and B/P-codoped Si NCs embedded in SiO_2 on the NC size. As previously demonstrated for P-doped Si NCs embedded in SiO_2 [38], the trend of the variation of E_f with respect to the dopant atom position may not change despite the change of the specific value of E_f when the NC size varies. Therefore, the similar preferential distribution of B and codoped B/P should occur as the NC size changes from 1.4 nm to a different one. It has been shown that the electronic structures of doped Si NCs critically depend on the doping-induced structural distortion [38,47]. When the NC size is $\geqslant$1.4 nm, Si NCs are less vulnerable to structural distortion [58–60]. Therefore, the current findings for the electronic structures of 1.4-nm B-doped and B/P-codoped Si NCs may be well qualitatively applied to larger Si NCs. It is clear that dedicated DFT studies are highly desired to quantitatively show the size effect for all kinds of doped Si NCs. With the continuous development of calculation methods and capacities this should be realized in the future. For now, current insights gained on the 1.4-nm B-doped and B/P-codoped Si NCs embedded in SiO_2 may encourage both theorists and experimentalists to further explore the great potential of Si NCs through controllable doping.

ACKNOWLEDGMENTS

Shanghai Supercomputer Center is acknowledged for providing computation resources. This study is mainly supported by the National Basic Research Program of China (Grant No. 2013CB632101), the Natural Science Foundation of China (NSFC) for Excellent Young Researchers program (Grant No. 61222404), and the NSFC-FWO program (Grants No. 61411130229 and No. 61511130264).

[1] T. Yu, F. Wang, Y. Xu, L. L. Ma, X. D. Pi, and D. Yang, Adv. Mater. **28**, 4912 (2016).

[2] R. J. Walters, G. I. Bourianoff, and H. A. Atwater, Nat. Mater. **4**, 143 (2005).

[3] F. Maier-Flaig, J. Rinck, M. Stephan, T. Bocksrocker, M. Bruns, C. Kubel, A. K. Powell, G. A. Ozin, and U. Lemmer, Nano Lett. **13**, 475 (2013).

[4] D. P. Puzzo, E. J. Henderson, M. G. Helander, Z. Wang, G. A. Ozin, and Z. Lu, Nano Lett. **11**, 1585 (2011).

[5] K. Y. Cheng, R. Anthony, U. R. Kortshagen, and R. J. Holmes, Nano Lett. **11**, 1952 (2011).

[6] L. Yao, T. Yu, L. X. Ba, H. Meng, X. Fang, Y. L. Wang, L. Li, X. Rong, S. Wang, X. Q. Wang, G. Z. Ran, X. D. Pi, and G. G. Qin, J. Mater. Chem. C **4**, 673 (2016).

[7] S. Y. Zhao, X. D. Pi, C. Mercier, Z. C. Yuan, B. Q. Sun, and D. Yang, Nano Energy **26**, 305 (2016).

[8] C.-Y. Liu, Z. C. Holman, and U. R. Kortshagen, Adv. Funct. Mater. **20**, 2157 (2010).

[9] Y. Ding, M. Sugaya, Q. Liu, S. Zhou, and T. Nozaki, Nano Energy **10**, 322 (2014).

[10] X. D. Pi, L. Zhang, and D. Yang, J. Phys. Chem. C **116**, 21240 (2012).

[11] J. Xu, S. H. Sun, Y. Q. Cao, P. Lu, W. Li, and K. J. Chen, Part. Part. Syst. Charact. **31**, 459 (2014).

[12] N. Liu, Z. Lu, J. Zhao, M. T. McDowell, H.-W. Lee, W. Zhao, and Y. Cui, Nat. Nanotechnol. **9**, 187 (2014).

[13] L. Zhong, J. Guo, and L. Mangolini, J. Power Sources **273**, 638 (2015).

[14] X. Cheng, S. B. Lowe, P. J. Reece, and J. J. Gooding, Chem. Soc. Rev. **43**, 2680 (2014).

[15] Y. L. Zhong, X. T. Sun, S. Y. Wang, F. Peng, F. Bao, Y. Y. Su, Y. Y. Li, S.-T. Lee, and Y. He, ACS Nano **9**, 5958 (2015).

[16] S. Park, E. Cho, D. Song, G. Conibeer, and M. A. Green, Sol. Energy Mater. Sol. Cells **93**, 684 (2009).

[17] A. R. Stegner, R. N. Pereira, K. Klein, R. Lechner, R. Dietmueller, M. S. Brandt, M. Stutzmann, and H. Wiggers, Phys. Rev. Lett. **100**, 026803 (2008).

[18] M. Kummer, J. P. Badillo, A. Schmitz, H. G. Bremes, M. Winter, C. Schulz, and H. Wiggers, J. Electrochem. Soc. **161**, A40 (2014).

[19] R. Lechner, H. Wiggers, A. Ebbers, J. Steiger, M. S. Brandt, and M. Stutzmann, Phys. Status Solidi RRL **1**, 262 (2007).

[20] H. Sugimoto, M. Fujii, M. Fukuda, K. Imakita, and S. Hayashi, J. Appl. Phys. **110**, 063528 (2011).

[21] A. Mimura, M. Fujii, S. Hayashi, D. Kovalev, and F. Koch, Phys. Rev. B **62**, 12625 (2000).

[22] Y. Hori, S. Kano, H. Sugimoto, K. Imakita, and M. Fujii, Nano Lett. **16**, 2615 (2016).

[23] P. Lu, W. Mu, J. Xu, X. Zhang, W. Zhang, W. Li, L. Xu, and K. Chen, Sci. Rep. **6**, 22888 (2016).

[24] S. Zhou, X. D. Pi, Z. Y. Ni, Y. Ding, Y. Y. Jiang, C. H. Jin, C. Delerue, D. Yang, and T. Nozaki, ACS Nano **9**, 378 (2015).

[25] X. D. Pi and C. Delerue, Phys. Rev. Lett. **111**, 177402 (2013).

[26] D. J. Rowe, J. S. Jeong, K. A. Mkhoyan, and U. R. Kortshagen, Nano Lett. **13**, 1317 (2013).

[27] N. J. Kramer, K. S. Schramke, and U. R. Kortshagen, Nano Lett. **15**, 5597 (2015).

[28] Z. Y. Ni, X. D. Pi, S. Zhou, T. Nozaki, B. Grandidier, and D. Yang, Adv. Opt. Mater. **4**, 700 (2016).

[29] S. Gutsch, J. Laube, D. Hiller, W. Bock, M. Wahl, M. Kopnarski, H. Gnaser, B. Puthen-Veettil, and M. Zacharias, Appl. Phys. Lett. **106**, 113103 (2015).

[30] D. König, S. Gutsch, H. Gnaser, M. Wahl, M. Kopnarski, J. Göttlicher, R. Steininger, M. Zacharias, and D. Hiller, Sci. Rep. **5**, 9702 (2015).

[31] T. Nakamura, S. Adachi, M. Fujii, H. Sugimoto, K. Miura, and S. Yamamoto, Phys. Rev. B **91**, 165424 (2015).

[32] M. Luppi and S. Ossicini, Phys. Status Solidi A **197**, 251 (2003).

[33] E. Holzenkämpfer, F. W. Richter, J. Stuke, and U. Voget-Grote, J. Non-Cryst. Solids **32**, 327 (1979).

[34] A. Stirling and A. Pasquarello, Phys. Rev. B **66**, 245201 (2002).

[35] D. L. Griscom, E. J. Friebele, K. J. Long, and J. W. Fleming, J. Appl. Phys. **54**, 3743 (1983).

[36] R. Guerra and S. Ossicini, J. Am. Chem. Soc. **136**, 4404 (2014).

[37] A. Carvalho, M. J. Rayson, and P. R. Briddon, J. Phys. Chem. C **116**, 8243 (2012).

[38] Z. Y. Ni, X. D. Pi, and D. Yang, Phys. Rev. B **89**, 035312 (2014).

[39] X. B. Chen, X. D. Pi, and D. Yang, J. Phys. Chem. C **115**, 661 (2011).

[40] K. Seino, F. Bechstedt, and P. Kroll, Phys. Rev. B **82**, 085320 (2010).
[41] X. D. Pi, R. Wang, and D. Yang, Chin. Phys. B **23**, 076102 (2014).
[42] B. Delley, J. Chem. Phys. **113**, 7756 (2000).
[43] Z. Y. Ni, X. D. Pi, and D. Yang, Chin. Phys. Lett. **29**, 077801 (2012).
[44] Z. Y. Ni, X. D. Pi, and D. Yang, RSC Adv. **2**, 11227 (2012).
[45] X. D. Pi, R. Wang, and D. Yang, J. Mater. Sci. Technol. **30**, 639 (2014).
[46] R. Wang, X. D. Pi, and D. Yang, J. Phys. Chem. C **116**, 19434 (2012).
[47] X. D. Pi, Z. Y. Ni, and D. Yang, J. Appl. Phys. **116**, 194304 (2014).
[48] R. A. Weeks, J. Non-Cryst. Solids **179**, 1 (1994).
[49] K. Seino, F. Bechstedt, and P. Kroll, Nanotechnology **20**, 135702 (2009).
[50] E. Degoli, S. Ossicini, G. Cantele, E. Luppi, R. Magri, D. Ninno, and O. Bisi, Phys. Status Solidi C **2**, 3354 (2005).
[51] A. Carvalho, S. Öberg, M. J. Rayson, and P. R. Briddon, Phys. Rev. B **86**, 045308 (2012).
[52] X. D. Pi, X. B. Chen, and D. Yang, J. Phys. Chem. C **115**, 9838 (2011).
[53] L. G. Wang and A. Zunger, Phys. Rev. B **66**, 161202 (2002).
[54] X. D. Pi, J. Nanomater. **2012**, 912903 (2012).
[55] K. Fujio, M. Fujii, K. Sumida, S. Hayashi, M. Fujisawa, and H. Ohta, Appl. Phys. Lett. **93**, 021920 (2008).
[56] R. Khelifi, D. Mathiot, R. Gupta, D. Muller, M. Roussel, and S. Duguay, Appl. Phys. Lett. **102**, 013116 (2013).
[57] M. Xie, D. S. Li, L. Chen, F. Wang, X. D. Zhu, and D. Yang, Appl. Phys. Lett. **102**, 123108 (2013).
[58] E. Degoli, G. Cantele, E. Luppi, R. Magri, D. Ninno, O. Bisi, and S. Ossicini, Phys. Rev. B **69**, 155411 (2004).
[59] X. Chen, X. D. Pi, and D. Yang, J. Phys. Chem. C **114**, 8774 (2010).
[60] X. Wang, R. Q. Zhang, S. T. Lee, T. Frauenheim, and T. A. Niehaus, Appl. Phys. Lett. **93**, 243120 (2008).